

ELECTRON HOLOGRAPHY AND ITS APPLICATIONS TO NANOWORLD OBSERVATION

AKIRA TONOMURA*)

Advanced Research Lab., Hitachi, Ltd.,
Hatoyama, Saitama 350-03, Japan

ABSTRACT

The wave nature of free electrons can now be used in the holographic process to observe the microscopic structure of objects through the advent of a "coherent" field-emission electron beam.

INTRODUCTION

Electron holography forms an image in two stages by using electron waves and light waves (Fig.1). First, in an electron microscope, an electron wave scattered by a specimen is recorded on film in the form of an interference pattern. The wavefront of the electron wave is then reproduced by impinging a laser beam on the film (hologram). The experiment can now be performed on an optical bench, and consequently what is impossible in the electron microscope is made possible by the optical technique.

Dennis Gabor, the inventor of holography, tried to significantly improve the resolution of the electron microscope by optically compensating for the unavoidable aberrations of the electron lenses (1).

Because holography uses the wave nature of light and electrons, the waves need high coherence and well-collimated wavefronts. In the field of light application, the laser was invented in 1960, and optical holography was developed soon afterwards (2). Application of electron technology produced the coherent electron gun in 1978, which, though imperfect, has been applied to holography (3). The field-emission electron gun has a 0.1 mm tungsten wire sharpened like a needle. The electron beam is extracted from the needle point by applying a voltage of several kilovolts. Because heating is not required, the electron velocities are uniform, and a bright point source is obtained. Thus, the field-emission electron microscope (Fig.2) has made possible the observation and recording of more than 1000 interference fringes, whereas only 100 were possible previously. This microscope has paved the way for electron holography.

*) The Electron Wavefront Project Organized by the Research Development Corporation of Japan

ELECTRON HOLOGRAPHY

Only the intensity of an electron beam can be observed with a general-purpose microscope. With electron holography, however, the phase distribution of the electron beam can also be observed as an image obtained by the interference microscope. This is done by superimposing optical plane waves on the optically reproduced image (Fig.3).

By using a technique peculiar to holography, the amplified phase distribution of the electron beam has been observed. As shown in Fig.1, in holography, in addition to the original image, a conjugate image, which is the amplitude of the complex conjugate, is produced. Additionally, in contrast to the interference microscope method which produces an interference pattern of plane waves and a reconstructed image, the conjugate image is superimposed instead of plane waves (Fig.3). Therefore, the phase difference is exactly doubled. As a result, the phase is amplified. By repeating this process the amplification can be increased. Currently, the phase shift of an electron wave that is one hundredth of a wavelength can be detected (4).

The effects of both the electric and magnetic fields can be observed with interference electron microscopy (5). This method leads to intuitive understanding, especially in cases of both magnetic samples and non-magnetic samples with thickness variations. Simple examples are shown in Fig.4.

When an electron beam is incident on a uniform magnetic field (see Fig.4(a)), the beam is deflected to the right by the Lorentz force which acts perpendicular to the direction of the magnetic field. When electrons are viewed as waves, the introduction of a wavefront perpendicular to the electron trajectory will suffice. The incident electron beam is a plane wave, but the outgoing beam becomes a tilted plane wave with the right side up. In other words, the wavefront appears to have revolved around a revolving axis, the magnetic line of force. From the contour map of this wavefront, we see that the contour lines follow the magnetic line of force. This is because the height of

the wavefront is the same along the magnetic line of force. Thus, when a magnetic field is observed as an interference electron micrograph, the contour fringe can be considered to be a magnetic line of force.

This interference fringe is also quantitative. A simple calculation verifies that a constant amount of minute magnetic flux, h/e , is flowing between adjacent contour fringes. A superconductive flux meter, SQUID, can measure the flux in units of $h/2e$ by using Cooper pair interference. The electron interference micrograph is formed due to interference of electrons, not Cooper pairs. In our case, the flux unit becomes h/e , since the electric charge of an electron is e instead of $2e$. The measurement principle is the same between the two cases.

When an electron penetrates a non-magnetic sample (see Fig.4(b)), it travels faster than in a vacuum, since it is accelerated by an inner potential V_0 (10-30 V). When the sample has a uniform inner potential V_0 and consequently has a uniform refractive index given by $n=1+V_0/2E$ (E :accelerating voltage of an electron beam), the transmitted electron wavefront is retarded in proportion to the thickness distribution. Therefore, the resultant contour map of the wavefront indicates the thickness contour map. Contour lines show every thickness change of $(2 E/V_0) \lambda$, where λ is the electron wavelength. When $E=100(\text{kV})$ and $V_0=10\text{-}30(\text{V})$, the thickness change for a 2π phase shift is $200\text{-}700 \text{ \AA}$.

The measurement sensitivity seems very low as compared with the extremely short wavelength of an electron beam. This is because the refractive index for an electron beam is very near to that of a vacuum. This is why the phase-amplification technique is indispensable in this field.

Recently, reflection electron holography has become feasible(6). Since an electron phase shift due to surface topography is measured by an extremely short electron wavelength, measurement sensitivity becomes very high.

APPLICATIONS OF ELECTRON HOLOGRAPHY

Thickness measurements at atomic dimensions

The first application introduced here is the thickness measurement of a specimen. An example of a beryllium particle is shown in Fig.5. Only the particle external shape is observed in reconstructed image (a). On the other hand, the thickness distribution can be directly observed from interference micrograph (b). One fringe spacing corresponds to a thickness change of 430 \AA . When phase-amplification is applied, a much more detailed thickness distribution can be observed, as shown in interference micrograph (c). The amplification rate is 32 times, and one fringe spacing corresponds to only 13 \AA .

One may doubt whether these fringes represent the thickness distribution precisely, or whether they are only interpolated without high precision. This problem was examined by observing surface steps (4), where the thickness change was already known. A 24-times amplified interference micrograph of a cleaved molybdenite thin film is shown in Fig.6. The phase distribution is displayed here as a deviation from regular fringes, i.e., an interferogram. Steps A, B and C in the micrograph correspond to the one, three and five layers of atomic surface steps, respectively. The thickness change at step A is 6.2 \AA (one-half of the c-axis spacing), and produces a phase shift of $2\pi/50$. This experiment shows that phase shift can be detected with an accuracy of the order of $2\pi/100$.

In transmission mode electron holography, surface topography can only be investigated through rather insensitive thickness measurements. However, we have recently demonstrated the feasibility of reflection holography using a Bragg-reflected beam. This means that surface topography can be directly measured to a precision of an electron wavelength (6).

This technique was used to quantitatively measure the surface undulation due to a single screw dislocation emerging on an atomically flat GaAs surface, as shown in Fig. 7. Although the interferogram is not phase-amplified, one fringe displacement

corresponds to only a 0.5 \AA height difference. A monoatomic step of 2 \AA can be seen until reaching the dislocation core. The surface topography surrounding the core can be observed at a glance. The surface undulation is similar to a spiral staircase. However, the staircase slope was found to be steep only in the opposite side of the step from the core.

Magnetic domain structure

Interference micrographs provide information about electromagnetic field distributions. Especially in magnetic field observation, this method has the following distinctive features: (1) Microscopic magnetic lines of force can be observed as overlapping contour lines in an in-focus electron micrograph. (2) Magnetic flux can be quantitatively measured in h/e units, since a constant flux of h/e flows between two contour lines.

An example is shown in Fig.8. The specimen is a fine particle cobalt (7). The thickness contour map appears in the periphery, showing that the thickness increases linearly to 550 \AA from the edges. Magnetic lines of force are observed in the inner region, where the thickness is uniform. The smooth rotating magnetization becomes observable at a glance even in such a particle.

A more practical application to high density magnetic recording (8) is shown in Fig.9. This is an important technology for information storage. The achievable density increases every year, and detailed observation of the recorded magnetization pattern is needed. A magnetic head was moved along a cobalt thin film and the magnetization bit pattern was recorded. The interference micrograph in Fig.9 shows a detailed distribution of the recorded magnetic lines of force. Recorded magnetization, the direction of which is indicated by arrows, can be observed as well as leaking magnetic fields. Magnetic fields distributed in space cannot be observed by Lorentz microscopy. Two oppositely directed magnetization streams merge and produce vortices similar to those produced by streams of water. Such observations helped to confirm the possibility of recording with a 0.15 \mu m bit

length.

Superconducting magnetic fluxons

A flux quantum, fluxon, is a minimum unit of flux when it is surrounded by a superconductor. The fluxon has evaded direct observation even though it is a key to the fundamental properties of superconductors and their practical use. This is because a flux, in addition to being extremely small, $h/2e (= 2 \times 10^{-45} \text{ Wb})$, is shaped like a very thin thread. Several methods have been developed to indirectly observe each thread of flux. In the Bitter method, magnetic powder is sprinkled on the superconductor's surface. The magnetic powder accumulates at positions of fluxons, forming an image of fluxons that can be observed by an electron microscope. Another method uses a scanning tunneling microscope (STM). In this method, a sharp needle scans the superconductor's surface. The tunneling current which flows between the surface and needle is measured, thus identifying the position of the fluxon.

We attempted to observe the fluxon by electron holography (9). The experimental arrangement is shown in Fig.10. A thin tungsten wire $30 \mu\text{m}$ in diameter is used as the superconducting specimen. Lead is evaporated onto one side of the wire. A magnetic field of several gauss or less is applied to the evaporated lead film. The specimen is cooled to 4.5K. In the weak magnetic field, the magnetic lines are excluded from the superconductor due to the Meissner effect. If the magnetic field is strong, the magnetic lines of force penetrate the superconductor in the form of flux quanta. By applying the electron beam to the specimen from above, we observed the magnetic lines of force through electron holography.

Figure 11 shows the single fluxon we observed when the superconductive film was $0.1 \mu\text{m}$ thick. In this figure, the phase difference is amplified by a factor of two. Therefore, one interference fringe corresponds to one fluxon. A single fluxon is captured in this photograph. The magnetic line of force is produced from an extremely small area of the lead surface, then

spread out into the free space. This is clearly shown in the photograph. A simple calculation proves that the magnetic field near the specimen's surface reaches as much as 1000 gauss even though the applied magnetic field is several gauss. A tiny solenoid is formed by the superconducting vortex current, resulting in a strong magnetic field.

Although this photograph may be sufficient to prove that the observed magnetic lines of force are definitely the fluxon, further confirmation was obtained by performing the following experiments.

When the temperature of the superconducting specimen exceeds the critical temperature, the magnetic lines disappear. This is because the superconducting state is destroyed, stopping the vortex current. This offers some proof that the observed magnetic lines were generated by the superconductive current.

There is more proof in that the fluxon corresponds exactly to $h/2e$. This was roughly understood from Fig.11. However, the flux value is more accurately obtained when amplified by phase amplification. This shows that the quantum flux value is $h/2e$ within an accuracy range of 10%.

In addition to observing isolated fluxon shown in Fig.11, we found another surprising result. A pair of fluxons were observed which were oriented in opposite directions and connected by magnetic lines of force (Fig.11, left). Even if this type of fluxons existed, the conventional methods were unable to detect it, because there was no way to determine the direction of the fluxons.

We do not yet understand why this pair was formed. However, the following explanation is feasible. When the specimen is cooled below the critical temperature, the lead is brought into the superconductive state. During cooling, however, the specimen experiences a state where the fluxon pair appears and disappears repeatedly. This was predicted by the Kosterlitz-Thouless theory. This phenomenon is peculiar to two-dimensional systems such

as thin films or layered structures. It has been pointed out that this phenomenon can occur in high-temperature superconductors. During cooling, a pair of fluxons are produced by thermal excitations, pinned by some imperfections in the superconductor and eventually frozen. The observed pair of fluxons were probably created in this way. If this explanation is correct, this photograph will be the first direct proof of the Kosterlitz-Thouless theory (10).

What happens when the thickness of the superconducting thin film is increased? Figure 12 shows the state of the magnetic lines of force when the thickness is 1 μm . We can see that the state is completely changed. Magnetic fluxes penetrate the superconductor in a bundle, not individually. The figure does not show any of the fluxon pairs.

Our explanation for this phenomena is as follows. Because the lead belongs to type-I superconductors, a strong magnetic field that is applied to it partially destroys the superconductive state in some parts of the specimen. (intermediate state). This state is shown in Fig.12. In this photograph, the magnetic lines of force penetrate the parts of the specimen where superconductivity is destroyed. However, since the other surrounding parts are still superconductive, the total amount of penetrating magnetic flux is an integral multiple of a flux quantum, $h/2e$.

Thin superconducting thin films (Fig.11) were an exception. In this case, lead behaves like a type-II superconductor and the flux penetrates the superconductor in the form of individual fluxons.

The Aharonov-Bohm effect (11)

Electron-holographic interferometry was effectively employed to test the existence or nonexistence of the Aharonov-Bohm (AB) effect (12) which had long been an object of controversy. The AB effect states that a phase shift is produced between two electron beams enclosing a magnetic flux even if they do not touch the flux, and implies the physical reality of gauge fields (vector

potentials) (13). This is the most fundamental postulate in the unified theory of all physical interactions in nature.

To help clarify, a new experiment on the AB effect was carried out to remove any overlap between electron beams and a magnetic flux (12). A tiny toroidal magnet was selected as a sample (Fig.13). The magnetic flux rotated inside the toroid and did not leak outside. This was confirmed by electron-holographic interferometry. The magnet was covered with a superconductive layer to completely confine the flux, and then with a copper layer for shielding from electron penetration. These samples were cooled down to 5K and the relative phase shift was measured between two electron beams passing through the hole and outside the toroid. Although the measurements were made for various magnetic flux values, only two kinds of interferograms were observed, as shown in Fig.14. The phase shift was either 0 or π .

This phase shift quantization implies that the magnetic flux is completely surrounded by the superconductor, and ensures that magnetic fields do not leak outside due to the Meissner effect. The observed phase shift of π under ideal conditions provides definitive evidence for the existence of the AB effect and also the physical reality of gauge fields.

CONCLUSIONS

Phase information has played an invaluable role in both image observation and fine measurements in light optics. However, the use of electron phase information has been limited. Since an electron beam has an extremely short wavelength of far less than 1 \AA , it can be expected to provide possible observation and measurement in atomic dimensions. This situation has improved somewhat since using of field-emission electron beams as coherent electron beams. This has opened the way to detect an electron phase shift down to $2\pi/50$ by using electron holography.

Although electron holography has not yet been fully de-

veloped, the author believes it has a bright future as an ultra-high precision measurement technology employed in both most advanced technology and most fundamental physics.

REFERENCES

1. D. Gabor: "Microscopy by Reconstructed Wavefronts",
Proc. R. Soc. London, Ser. A 197, 454-487(1949).
D. Gabor: "Microscopy by Reconstructed Wavefronts II",
Proc. Phys. Soc. London, Sec. B 64, 449-469(1951).
2. E. N. Leith and J. Upatnieks: "Reconstructed Wavefronts and
Communication Theory", J. Opt. Soc. Am. 52, 1123-1130(1962).
3. A. Tonomura, T. Matsuda, J. Endo, H. Todokoro and T. Komoda:
"Development of a Field Emission Electron Microscope",
J. Electron Microsc. 28, 1-11(1979).
4. A. Tonomura, T. Matsuda, T. Kawasaki, J. Endo and N. Osakabe:
"Sensitivity-Enhanced Electron-Holographic Interferometry and
Thickness-Measurement Applications at Atomic Scale", Phys.
Rev. Lett. 54, 60-62(1985).
5. For example: A. Tonomura: "Application of electron holography",
Rev. Mod. Phys. 59, 637-669(1987); A. Tonomura:
"Electron holography: A new view of the microscopic",
Physics Today 22, 22-29(April 1990).
6. N. Osakabe, J. Endo, T. Matsuda, A. Tonomura and A. Fukuhara:
"Observation of Surface Undulation Due to a Single-Atomic
Shear of a Dislocation by Reflection Electron Holography"
Phys. Rev. Lett. 62 2969-2972(1989).
7. A. Tonomura, T. Matsuda, J. Endo, T. Arai, K. Mihama: "Direct
Observation of Fine Structures of Magnetic Domain Walls by
Electron Holography", Phys. Rev. Lett, 44, 1430-1433(1980).

8. N. Osakabe, K. Yoshida, Y. Horiuchi, T. Matsuda, H. Tanabe, T. Okuwaki, J. Endo, H. Fujiwara and A. Tonomura: "Observation of recorded magnetization pattern by electron holography", Appl. Phys. Lett. 42, 746-748(1983).
9. T. Matsuda, S. Hasegawa, M. Igarashi, T. Kobayashi, M. Naito, H. Kajiyama, J. Endo, N. Osakabe, A. Tonomura and R. Aoki: "Magnetic Field Observation of a Single Flux Quantum by Electron-Holographic Interferometry", Phys. Rev. Lett., 62, 2519-2522(1989).
10. J. M. Kosterlitz and D. Thouless: "Ordering, metastability and phase transitions in two-dimensional systems", J. Phys. C6, 1181-1203(1973); B. I. Halperin and D. R. Nelson: "Resistive Transition in Superconducting Films", J. Low Temp. Phys. 36, 599-616(1979).
11. Y. Aharonov and D. Bohm: "Significance of Electromagnetic Potentials in Quantum Theory", Phys. Rev. 115, 485-491(1959).
12. A. Tonomura, T. Matsuda, R. Suzuki, A. Fukuhara, N. Osakabe, H. Umezaki, J. Endo, K. Shinagawa, Y. Sugita and H. Fujiwara: "Observation of Aharonov-Bohm Effect by Electron Holography", Phys. Rev. Lett. 48, 1443-1446(1982); A. Tonomura, N. Osakabe, T. Matsuda, T. Kawasaki, J. Endo, S. Yano and H. Yamada: "Evidence for Aharonov-Bohm Effect with Magnetic Field Completely Shielded from Electron Wave" Phys. Rev. Lett. 56, 792-795(1986); M. Peshkin and A. Tonomura: "The Aharonov-Bohm Effect", Lecture Notes in Physics, Vol. 340 (Springer-Verlag, 1989).
13. T. T. Wu and C. N. Yang: "Concept of nonintegrable phase factors and global formulation of gauge fields", Phys. Rev. D12, 3845-3857(1975).

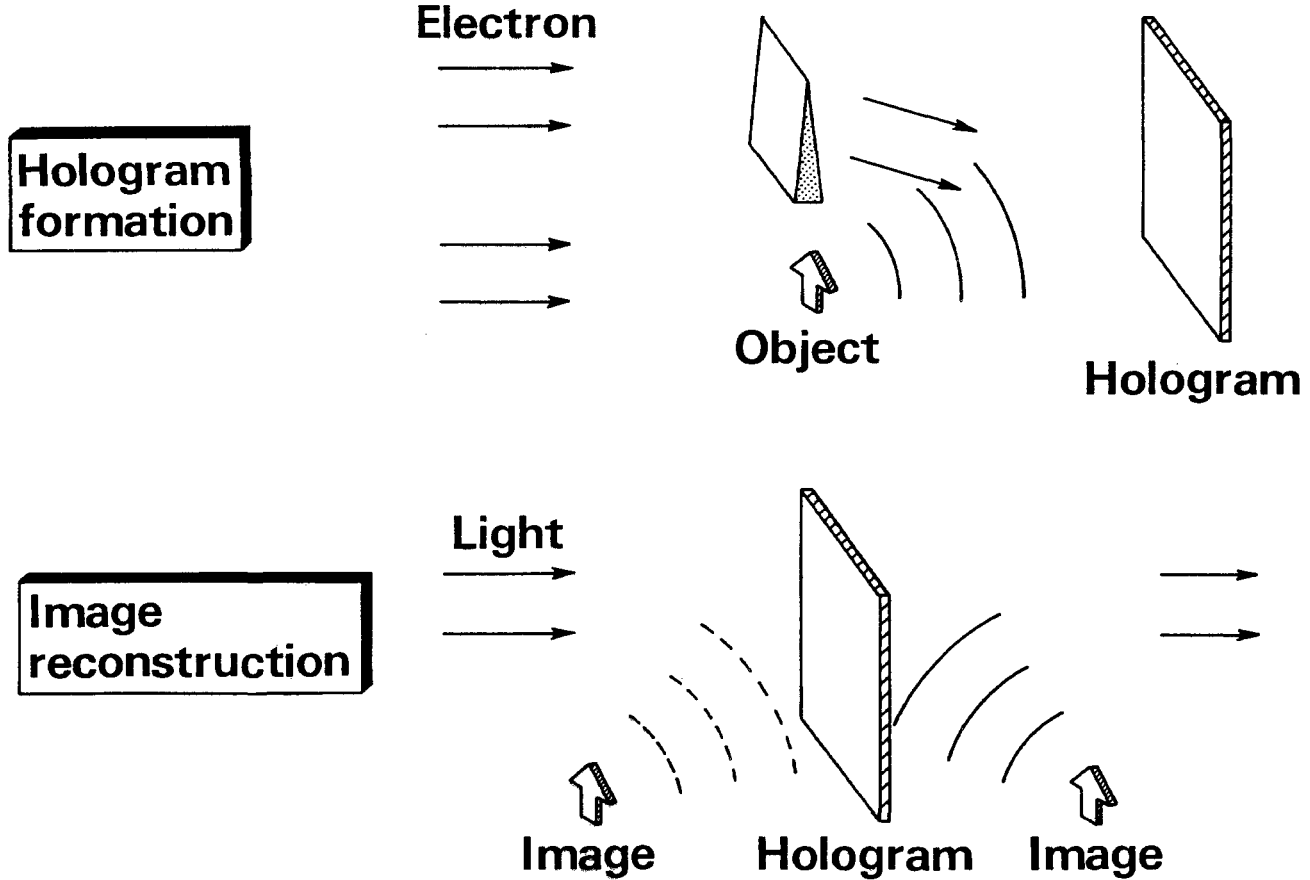


Figure 1. Principle behind electron holography.

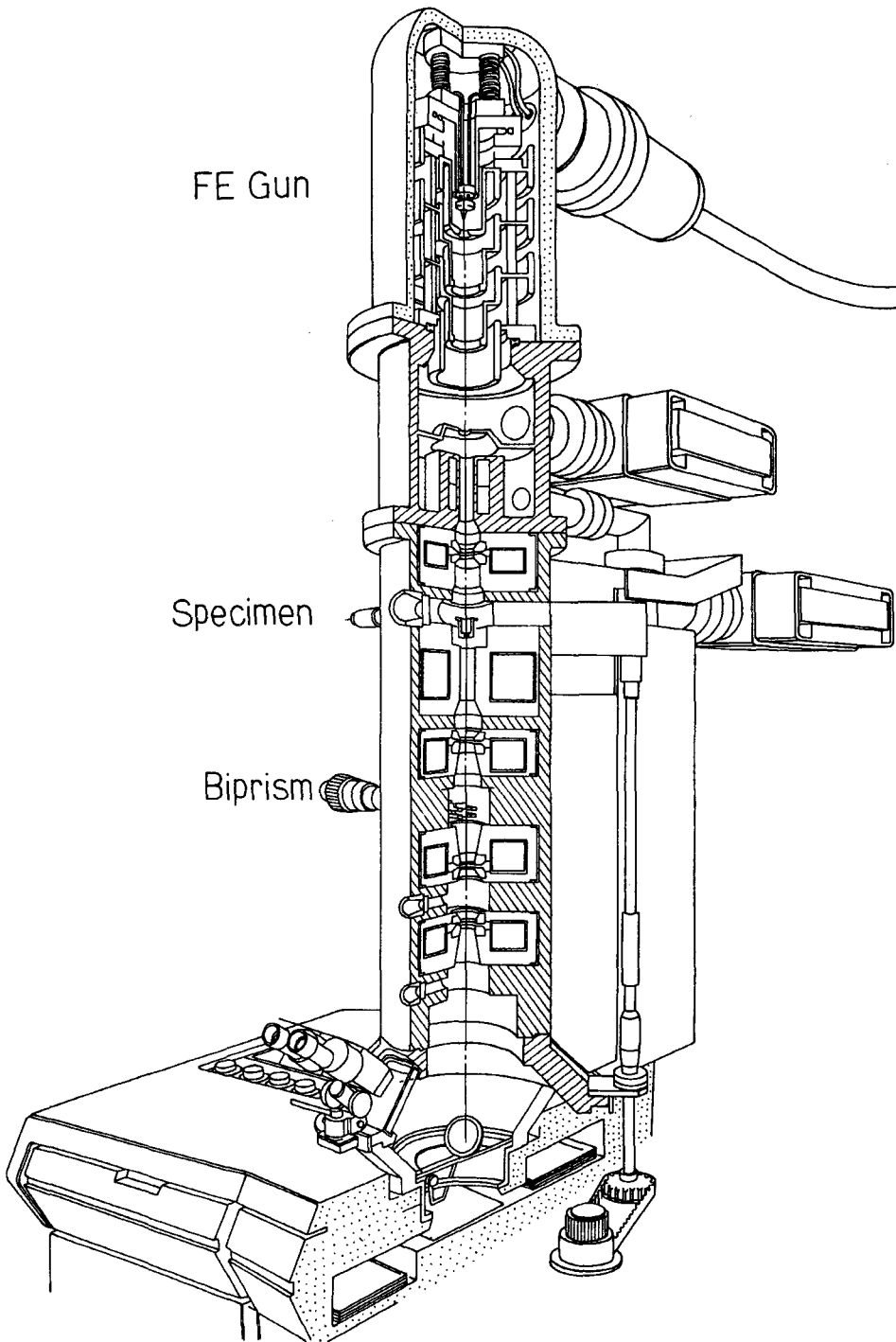


Figure 2. Cross-sectional diagram of a field-emission electron microscope.

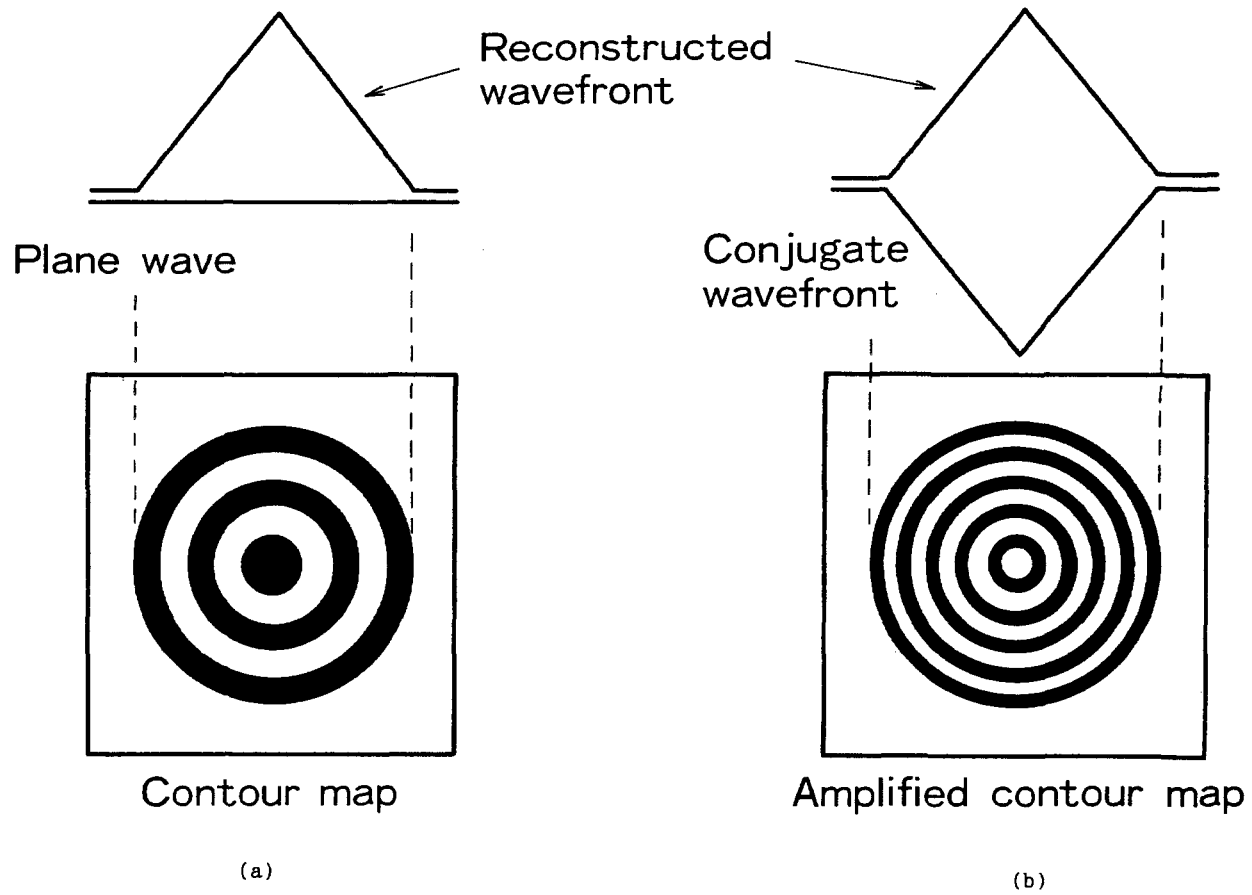


Figure 3. Principle behind phase amplification.

(a) Conventional interference micrograph

(b) Interference micrograph phase-amplified twice

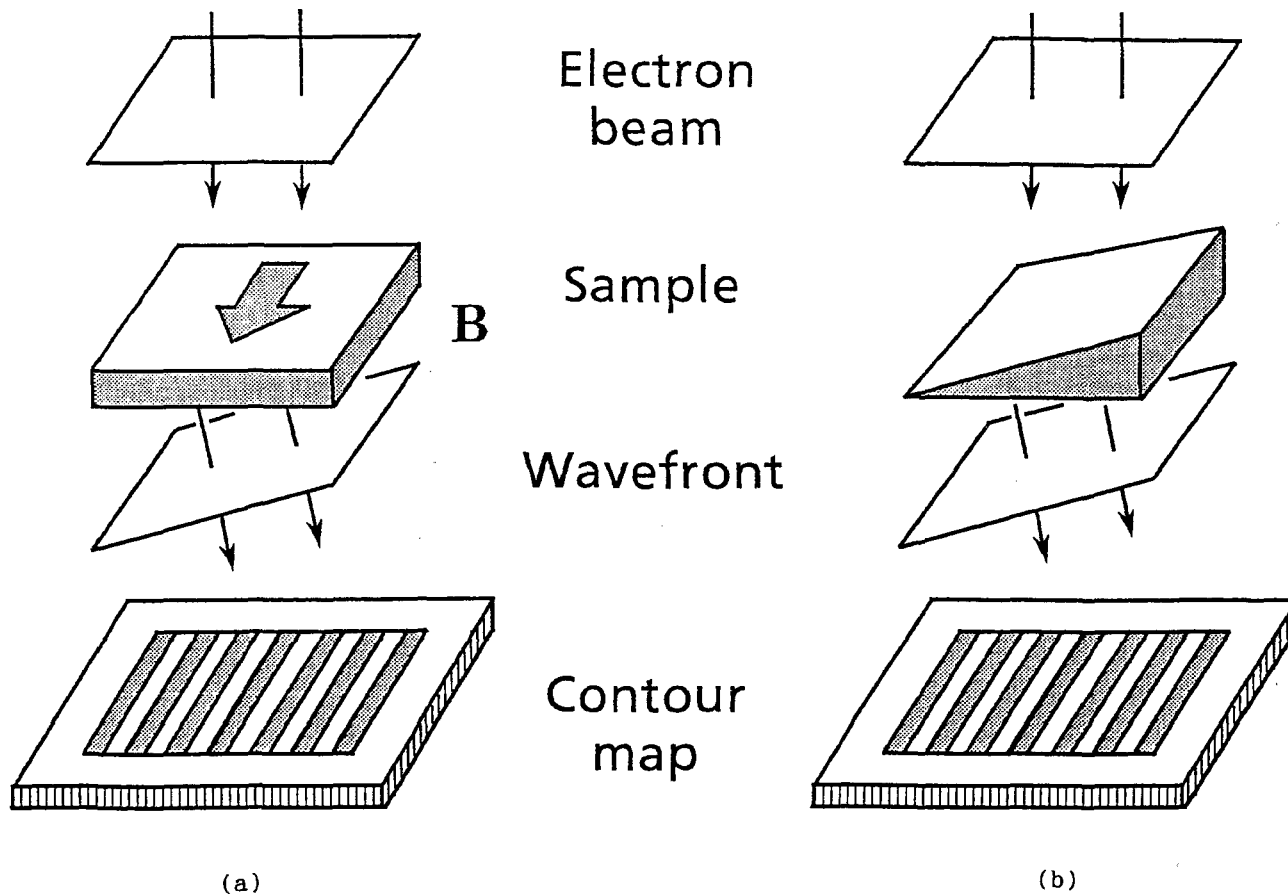


Figure 4. Principle behind electromagnetic-field observation.

(a) Magnetic lines of force

(b) Thickness distribution

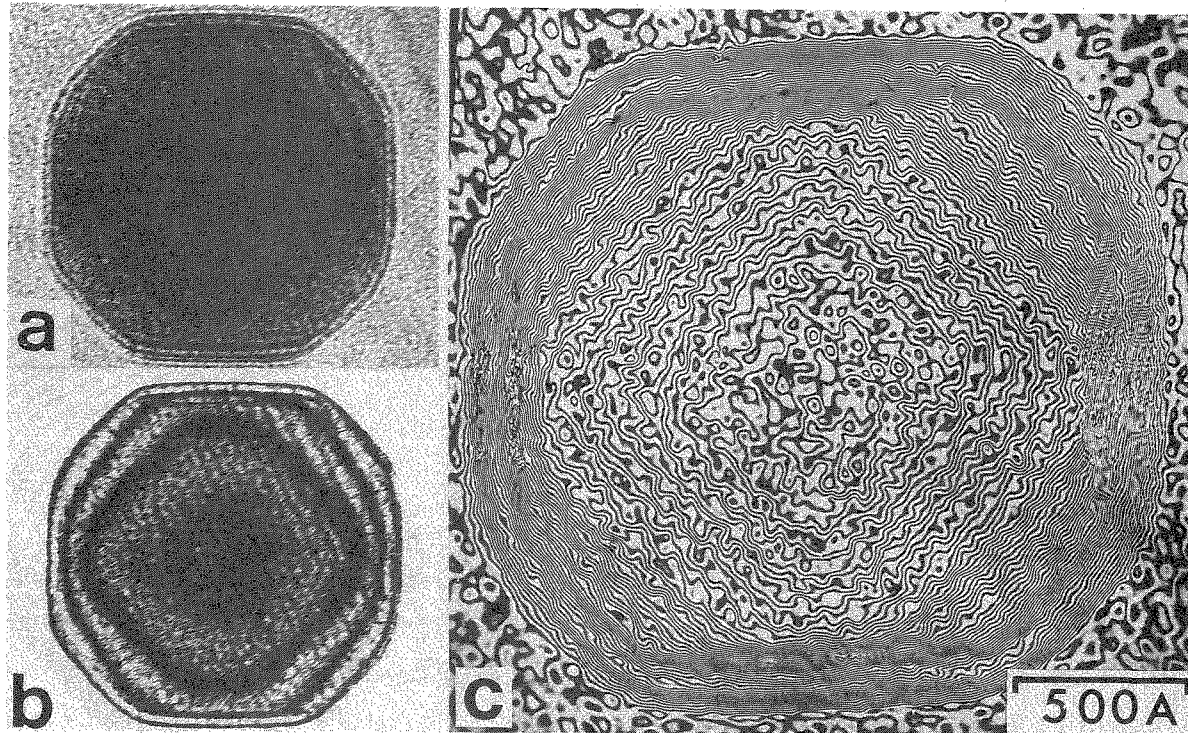


Figure 5. Interference micrographs of fine particle Beryllium.

(a) Reconstructed image, i.e. electron micrograph

(b) Conventional contour map

(c) Contour map phase-amplified 32 times

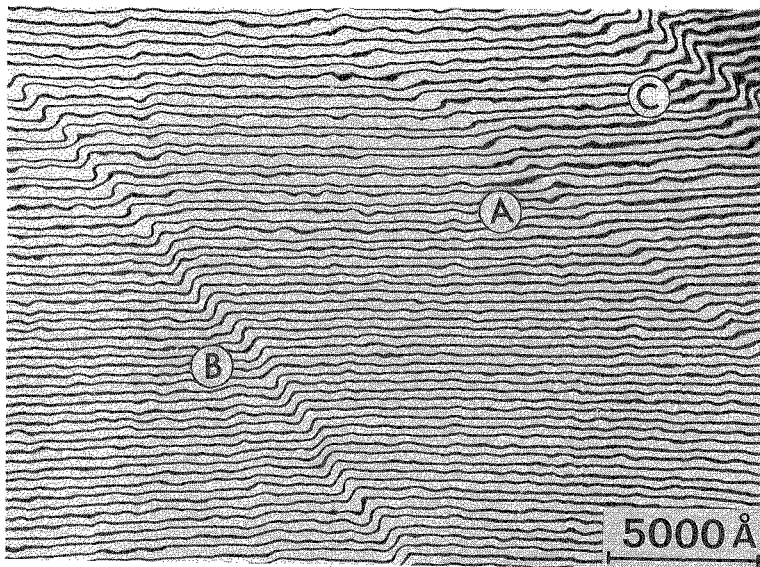


Figure 6. Interference micrographs of thin film molybdenite.
(Phase amplification: x 24)

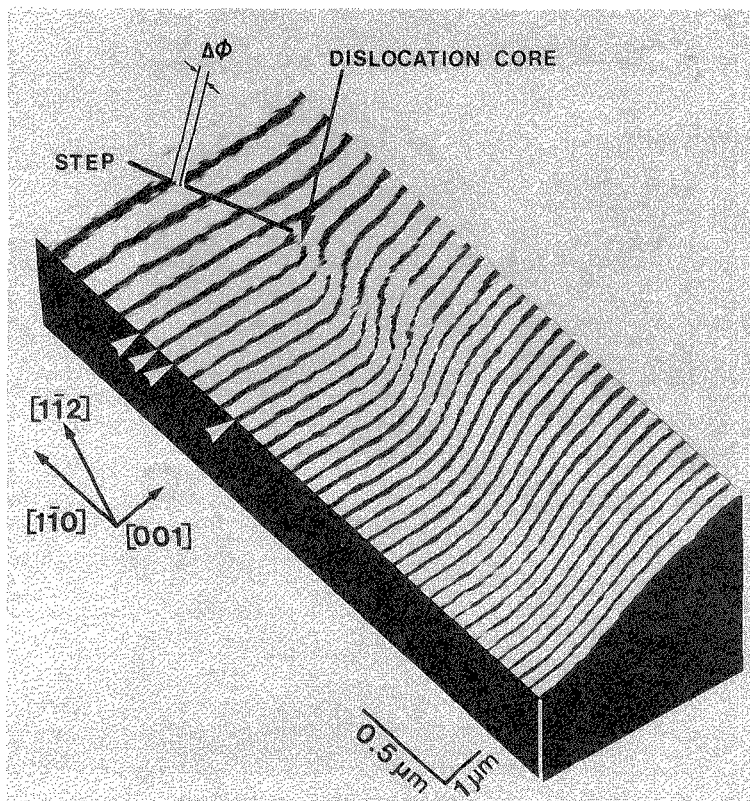


Figure 7. Interference micrograph of GaAs (110) surface.

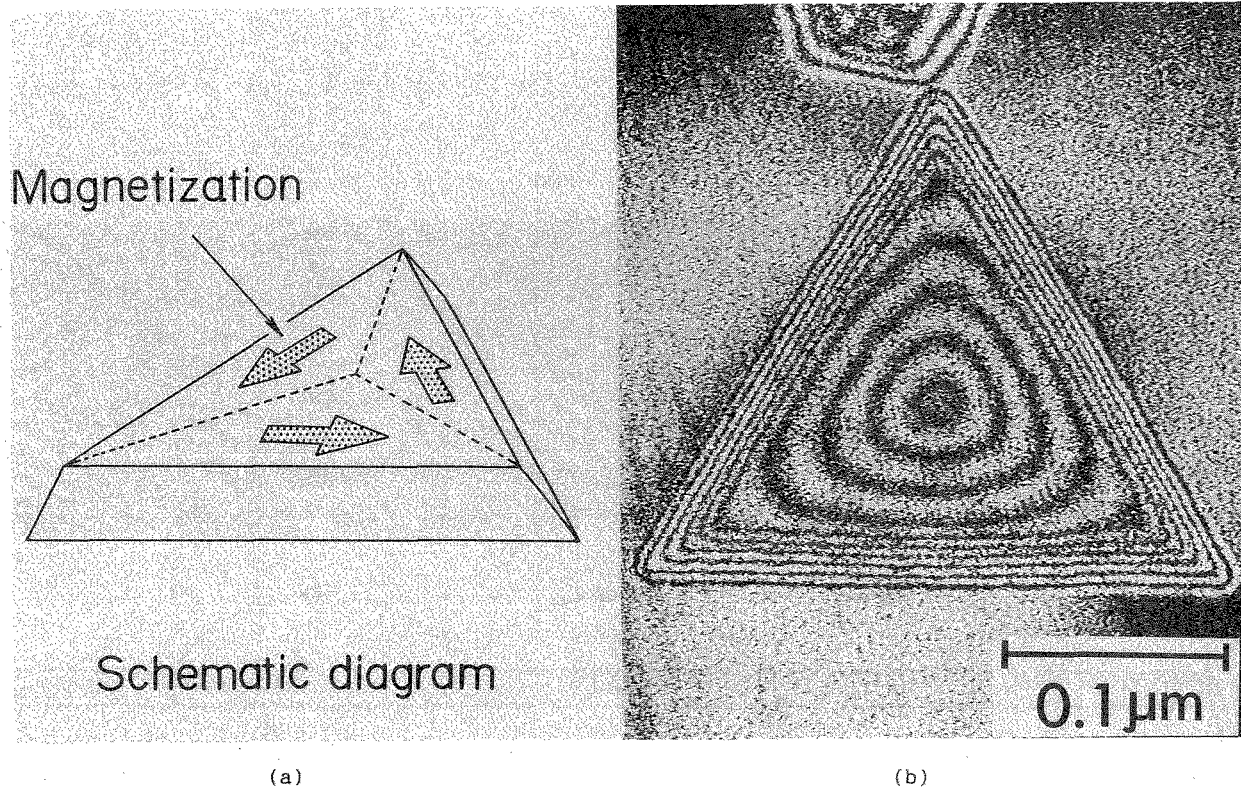


Figure 8. Interference micrograph of fine particle Cobalt.

(a) Schematic

(b) Interference micrograph

(Phase amplification: x 2)

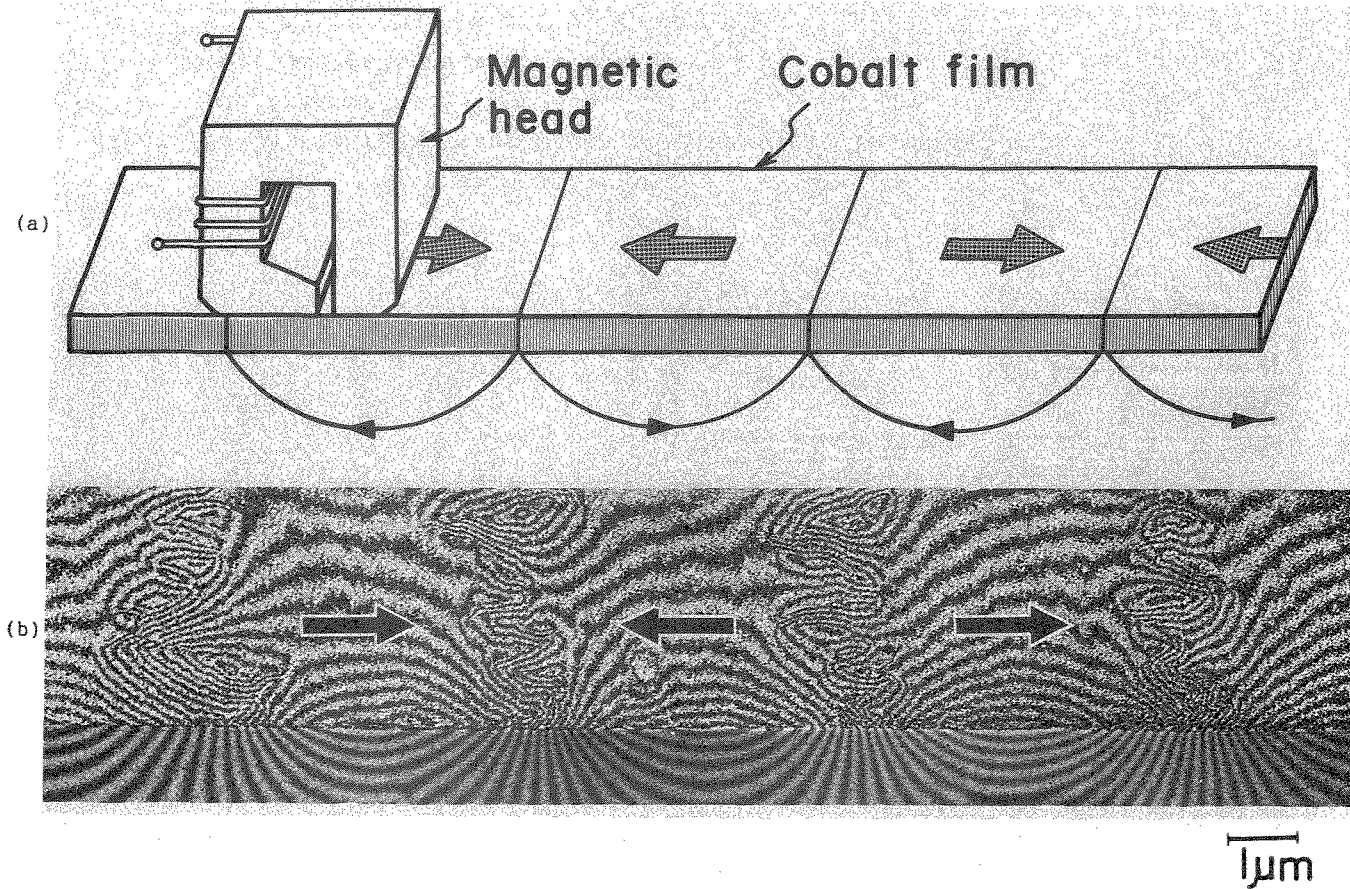


Figure 9. Magnetically recorded Co thin film.

(a) Recording method

(b) Contour map

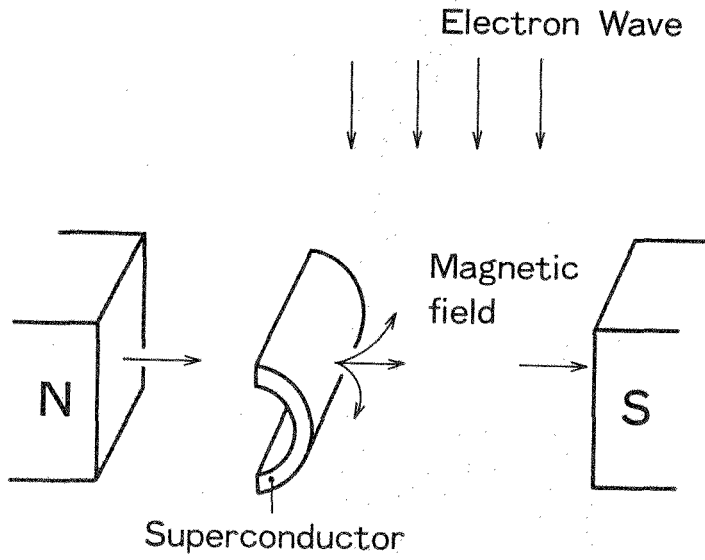


Figure 10. Experiment of fluxon observation.

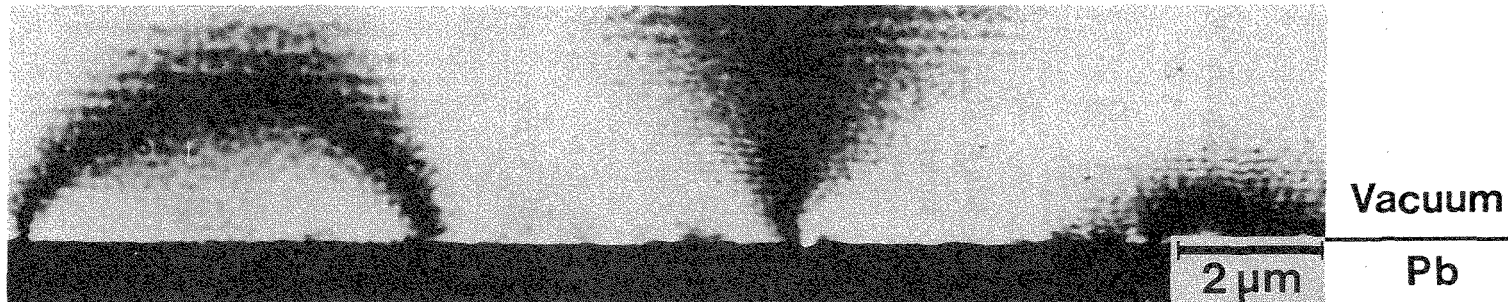


Figure 11. Magnetic lines of force penetrating lead film 0.2 μm thick (Phase difference amplification: x 2).

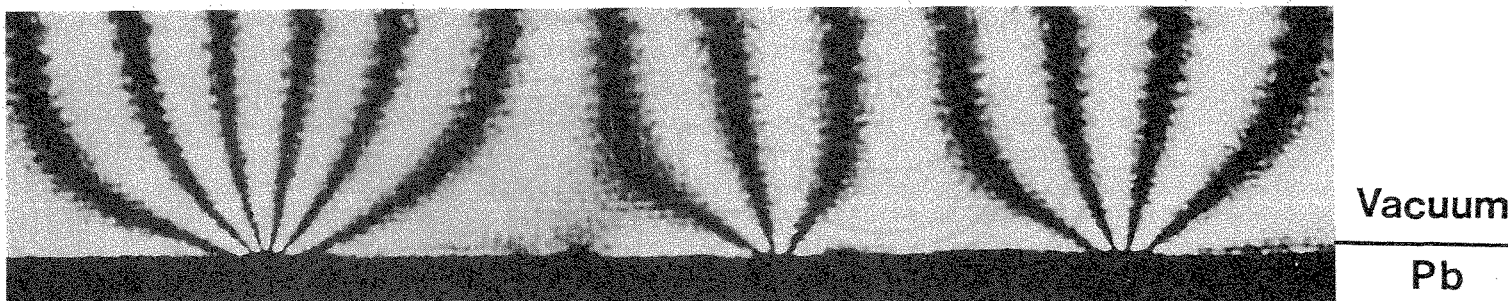
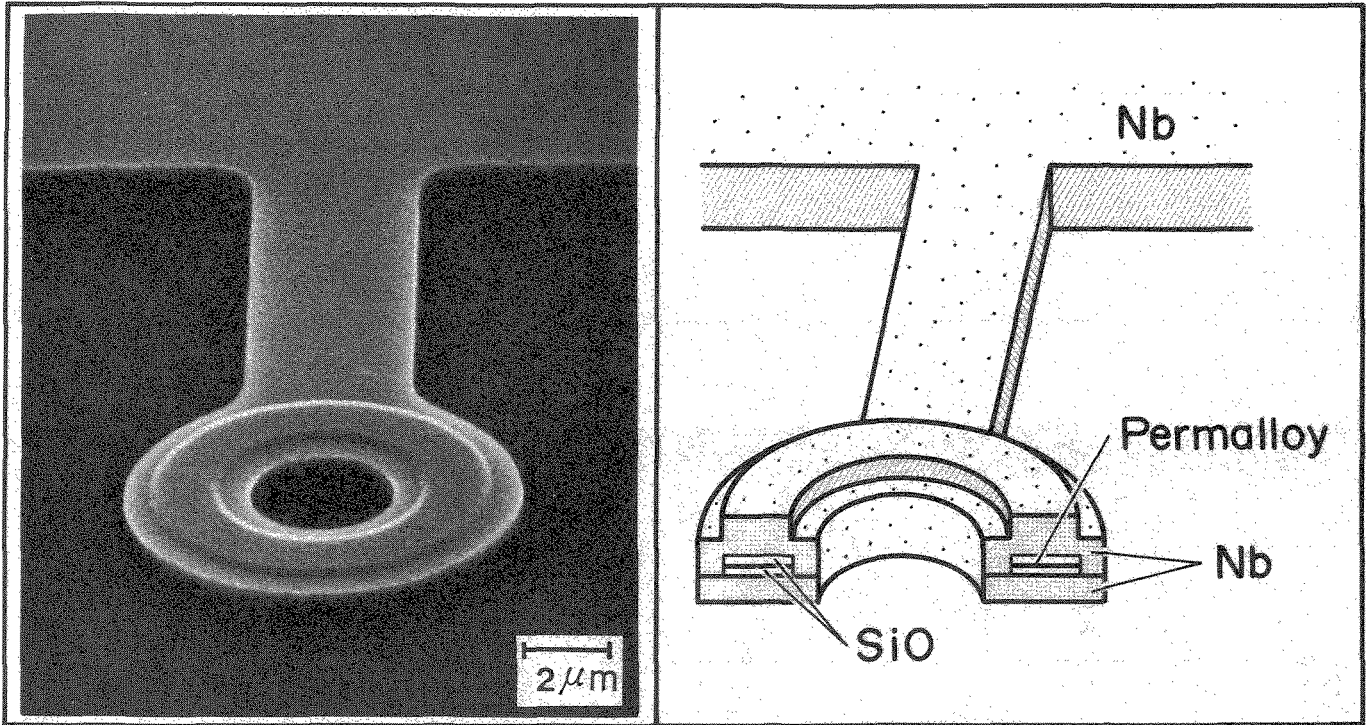


Figure 12. Magnetic lines of force penetrating lead film $1 \mu\text{m}$ thick (Phase difference amplification: $\times 2$).



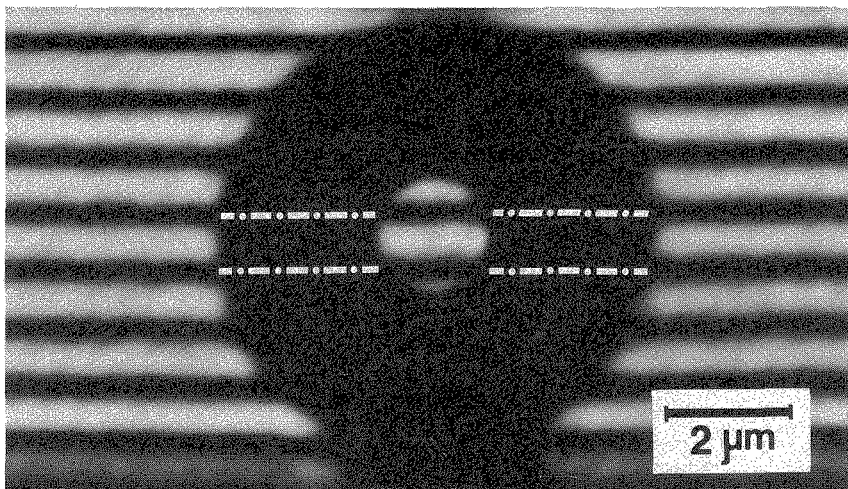
(a)

(b)

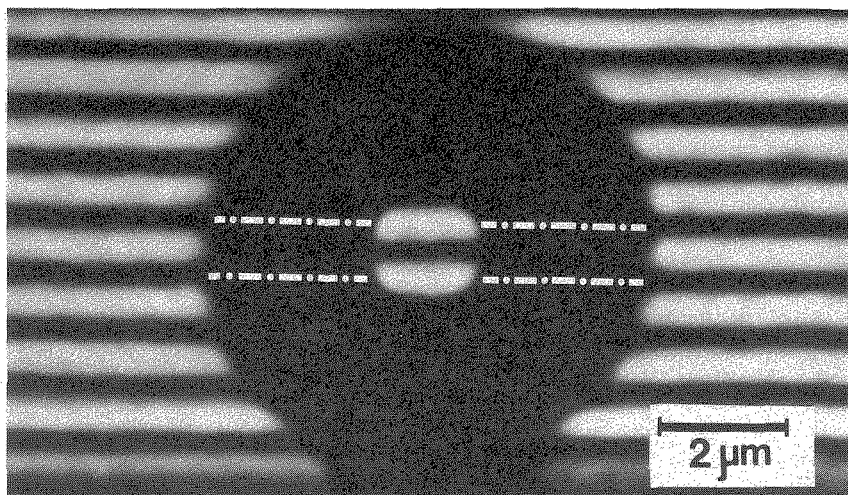
Figure 13. Toroidal magnets completely covered with superconducting layers.

(a) Scanning electron micrograph

(b) Schematic



(a)



(b)

Figure 14. Electron interference patterns of toroidal magnets.

(a) Phase shift = 0

(b) Phase shift = π